Inorganic Chemistry

Article

pubs.acs.org/IC

Structure, Phase Transition, and Controllable Thermal Expansion Behaviors of $Sc_{2-x}Fe_xMo_3O_{12}$

Meimei Wu,*[†] Xinzhi Liu,[†] Dongfeng Chen,*[†] Qingzhen Huang,[‡] Hui Wu,[‡,§] and Yuntao Liu[†]

[†]China Institute of Atomic Energy, Beijing 102413, China

[‡]NIST Center for Neutron Research, NIST, Gaithersburg, Maryland 20899, United States

[§]Department of Materials Science and Engineering, University of Maryland, College Park, Maryland 20742, United States

Supporting Information

ABSTRACT: The crystal structures, phase transition, and thermal expansion behaviors of solid solutions of $Sc_{2-x}Fe_xMo_3O_{12}$ ($0 \leq x \leq 2$) have been examined using X-ray diffraction (XRD), neutron powder diffraction (NPD), and differential scanning calorimetry (DSC). At room temperature, samples crystallize in a single orthorhombic structure for the compositions of $x < 0.6$ and monoclinic for $x \geq 0.6$, respectively. DSC results indicate that the phase transition temperature from monoclinic to orthorhombic structure is enhanced by increasing the Fe^{3+} content. High-temperature XRD and NPD results show that $Sc_{1.3}Fe_{0.7}Mo_3O_{12}$ exhibits near zero thermal expansion, and the volumetric coefficients of thermal expansion derived from XRD and NPD are 0.28×10^{-6} °C^{-1} (250−800 °C) and 0.65×10^{-6} °C^{-1} (227−427 °C), respectively. NPD results of $Sc_2Mo_3O_{12}$ ($x = 0$) and $Sc_{1.3}Fe_{0.7}Mo_3O_{12}$ ($x = 0.7$) indicate that Fe substitution for Sc induces reduction of the mean Sc(Fe)−Mo nonbond distance and the different thermal variations of Sc(Fe)−O5−Mo2 and Sc(Fe)−O3−Mo2 bond angles. The correlation between the displacements of oxygen atoms and the variation of unit cell parameters was investigated in detail for $Sc_2Mo_3O_{12}$.

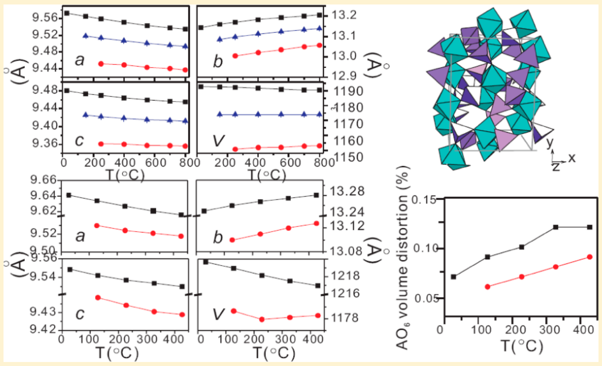

1. INTRODUCTION

Negative thermal expansion (NTE) materials have attracted considerable interest in recent years, because of their potential applications in electrical, optical, and high-temperature devices.[1,2] A number of NTE systems, including the ZrW_2O_8, AM_2O_7, $A_2M_3O_{12}$, and Mn_3AN families, have been discovered.[1−10] Among these families, the $A_2M_3O_{12}$ family presents great chemical flexibility; A^{3+} can be a trivalent ion ranging from Al^{3+} to Dy^{3+}, while M^{6+} may be W^{6+} or Mo^{6+}. $A_2M_3O_{12}$ crystallizes in a monoclinic or orthorhombic structure, depending on the A^{3+} size, and are composed of AO_6 octahedra and MO_4 tetrahedra. Partial compounds undergo a phase transition between the monoclinic and orthorhombic phases,[11] but only orthorhombic compounds could exhibit NTE. The mechanism of NTE is attributed to the rocking motion of the polyhedra, which is related to the transverse vibrations of A−O−M linkages.[1,2] Delicate mechanisms to control the thermal expansion properties of materials have been extensively investigated. Previous studies have verified that the coefficient of thermal expansion (CTE) of $A_2M_3O_{12}$ can be adjusted through partial substitution of the A^{3+} cation.[12−16] However, the effect of substitution on the crystal structure and thermal expansion behavior needs further study.

To comprehensively understand the correlation between the crystal structure and thermal expansion behavior, solid solutions with the general formula $Sc_{2-x}Fe_xMo_3O_{12}$ ($0 \leq x \leq 2$) were synthesized. $Sc_2Mo_3O_{12}$[17] and $Fe_2Mo_3O_{12}$[13,18] crystallize in a monoclinic structure ($P2_1/a$) at and below −95 and 499 °C, respectively, and transform to an orthorhombic structure ($Pnca$) upon heating. Orthorhombic $Sc_2Mo_3O_{12}$[19] exhibits NTE in the temperature range of 25 to 800 °C, with a volumetric CTE (α_v) of -7.00×10^{-6} °C^{-1}; in contrast, orthorhombic $Fe_2Mo_3O_{12}$[13] demonstrates positive thermal expansion from 540 to 800 °C, with an α_v value of 3.42 $\times$ 10^{-6} °C^{-1}. Therefore, the thermal expansion of $Sc_{2-x}Fe_xMo_3O_{12}$ solid solutions could be controlled by carefully adjusting the Sc^{3+}/Fe^{3+} ratio. In this paper, the effects of Fe substitution for Sc on the crystal structure, phase transition, and thermal expansion of the resultant solid solutions were systematically studied using X-ray diffraction (XRD), neutron powder diffraction (NPD), and differential scanning calorimetry (DSC).

2. EXPERIMENTAL SECTION

All $Sc_{2-x}Fe_xMo_3O_{12}$ ($0 \leq x \leq 2$) samples were prepared through the solid-state method. Stoichiometric amounts of Sc_2O_3 (purity 99.95%), Fe_2O_3 (purity 99.99%), and MoO_3 (purity ≥99.0%) were weighed, mixed, and homogenized in an agate mortar. The reactants were

Received: June 3, 2014
Published: August 20, 2014

ACS Publications © 2014 American Chemical Society

dx.doi.org/10.1021/ic501271t | Inorg. Chem. 2014, 53, 9206−9212

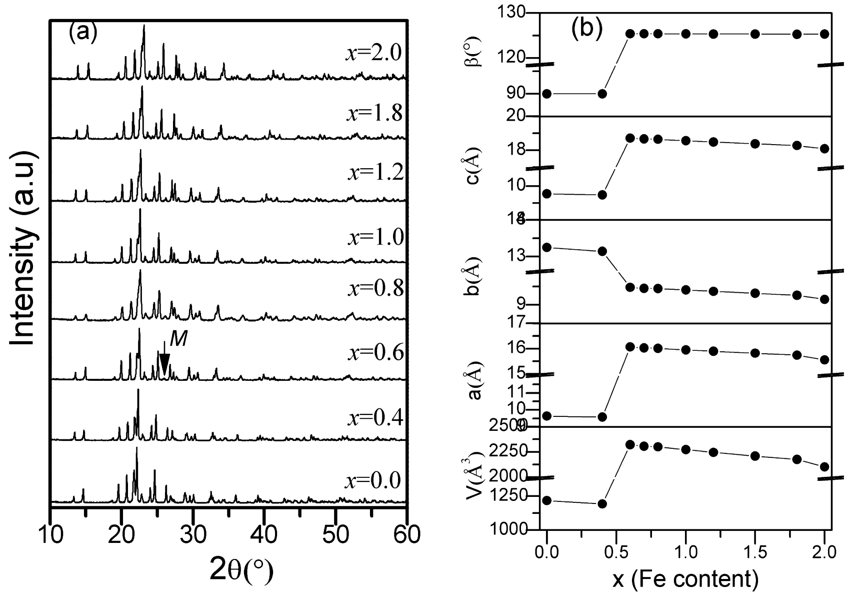

Figure 1. (a) XRD patterns and (b) cell parameters of $Sc_{2-x}Fe_xMo_3O_{12}$ ($0 \leq x \leq 2$) at room temperature.

calcined in air in alumina crucibles at 800 to 850 °C for 48 h with intermittent regrinding and then cooled in the furnace.

Phase identification of the $Sc_{2-x}Fe_xMo_3O_{12}$ compounds was performed through XRD using a Bruker D8 Advanced diffractometer with Cu Kα radiation. The thermal expansion behavior of $Sc_{2-x}Fe_xMo_3O_{12}$ was investigated using a PAN X'Pert PRO MPD XRD with an X'Celerator detector and an Anton Parr high-temperature attachment. High-temperature XRD data for $Sc_{2-x}Fe_xMo_3O_{12}$ (x = 0.4, 0.7, and 1.2) were recorded at 25, 150, 250, 400, 550, 700, and 800 °C in the 2θ range of 10° to 80°. The sample was heated to the desired temperature on a platinum strip at a rate of 30 °C/min and kept for 5 min for equilibration before the XRD data were collected. A detailed study of the solid solution structure was carried out with the Rietveld method using Fullprof software.[20] Atomic parameters for monoclinic and orthorhombic structure refinement were obtained from those reported for $Fe_2Mo_3O_{12}$[18] and $Sc_2Mo_3O_{12}$,[17] respectively.

NPD patterns for $Sc_{2-x}Fe_xMo_3O_{12}$ (x = 0 and 0.7) were collected from 27 to 427 °C using a high-resolution neutron powder diffractometer (BT-1) at the NIST Center for Neutron Research (NCNR). NPD data were collected with a step size of 0.05° in the 2θ range of 3−168°. A Cu (311) monochromator was used to produce monochromatic neutron beams with a wavelength of 1.5403 Å. Collimators with horizontal divergences of 15′, 20′, and 7′ were used before and after the monochromator and after the sample, respectively. The positions of the reflections and lattice parameters were calculated using the General Structure Analysis System (GSAS).[21]

Differential scanning calorimetry measurement was performed on a TA Instruments Q100 system under a nitrogen atmosphere to investigate the phase transition of $Sc_{1.3}Fe_{0.7}Mo_3O_{12}$ and $Sc_{0.8}Fe_{1.2}Mo_3O_{12}$ from 25 to 400 °C at a rate of 10 °C/min.

3. RESULTS AND DISCUSSION

3.1. Phase Formation. Figure 1a shows the XRD patterns of the $Sc_{2-x}Fe_xMo_3O_{12}$ ($0 \leq x \leq 2$) samples at room temperature. All the samples show a single phase because of the relatively small difference between the Sc^{3+} (0.73 Å) and Fe^{3+} (0.64 Å) radii. XRD patterns indicate that samples adopt a $Sc_2Mo_3O_{12}$-type orthorhombic structure (*Pnca*) for $x < 0.6$ and an $Fe_2Mo_3O_{12}$-type monoclinic structure ($P2_1/a$) for $x \geq 0.6$. The difference in the characteristic diffraction peaks between the monoclinic and orthorhombic structures is shown in Figure 1a (indicated by "*M*"). The dependence of the lattice parameters on the Fe content derived from Rietveld refinement is shown in Figure 1b. The cell parameters *a*, *b*, *c*, and volume *V* of both the monoclinic and orthorhombic $Sc_{2-x}Fe_xMo_3O_{12}$ linearly decrease as Fe content increases. This result can be expected due to the smaller ionic radius of Fe^{3+} compared with that of Sc^{3+}.

3.2. Phase Transition. Most $A_2Mo_3O_{12}$ compounds have been reported to demonstrate a phase transition from the monoclinic to orthorhombic structure upon heating.[11] The transition temperatures for $Sc_2Mo_3O_{12}$[17] and $Fe_2Mo_3O_{12}$[13] have been reported to be −95 and 499 °C, respectively. In the present study, the transition temperature of $Sc_{1.3}Fe_{0.7}Mo_3O_{12}$ and $Sc_{0.8}Fe_{1.2}Mo_3O_{12}$ detected using DSC is 112 and 241 °C, respectively. Partial substitution of Fe^{3+} for Sc^{3+} notably inhibits the phase transition from monoclinic to orthorhombic structure. Previous studies[11,22,23] suggested that the phase transition temperature increases as the electronegativity of the A^{3+} cation increases. Since the electronegativity of Fe^{3+} (1.83) is larger than that of Sc^{3+} (1.36), the phase transition of $Sc_{2-x}Fe_xMo_3O_{12}$ occurs at higher temperatures with increasing Fe content. As a result, the samples $Sc_{2-x}Fe_xMo_3O_{12}$ when $x \geq 0.6$ exhibit a monoclinic structure at room temperature.

3.3. Thermal Expansion Property. *3.3.1. High-Temperature XRD.* The thermal expansion properties of $Sc_{2-x}Fe_xMo_3O_{12}$ (x = 0.4, 0.7, and 1.2) were investigated using high-temperature XRD. The $Sc_{1.6}Fe_{0.4}Mo_3O_{12}$ sample retains an orthorhombic structure from 25 to 800 °C. $Sc_{1.3}Fe_{0.7}Mo_3O_{12}$ and $Sc_{0.8}Fe_{1.2}Mo_3O_{12}$ exhibit a monoclinic structure at low temperature and transform to an orthorhombic structure above phase transition temperature. Both monoclinic $Sc_{1.3}Fe_{0.7}Mo_3O_{12}$ and $Sc_{0.8}Fe_{1.2}Mo_3O_{12}$ exhibit positive thermal expansion, as observed in the other monoclinic systems.[17,24]

Variations in the cell parameters *a*, *b*, *c*, and volume *V* of orthorhombic $Sc_{2-x}Fe_xMo_3O_{12}$ (x = 0.4, 0.7, and 1.2) with temperature are shown in Figure 2. All of the *a*- and *c*-axes decrease upon heating throughout the temperature range; in contrast, the *b*-axis increases as the temperature increases. The small errors in the lattice parameters warrant a reliable determination of CTE. The cooperative effect of axial contraction or expansion leads to the different thermal

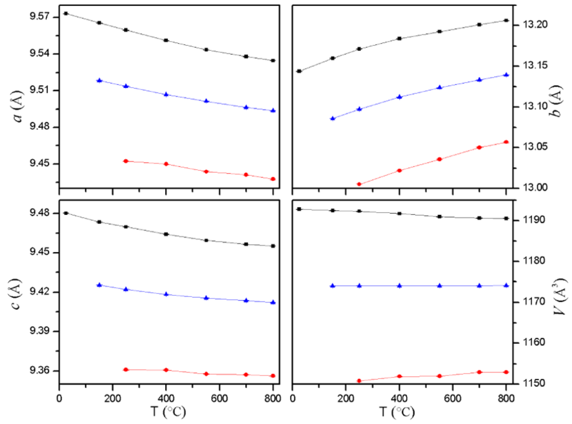

Figure 2. Variations of cell parameters a, b, c, and volume V with temperature for orthorhombic samples $Sc_{2-x}Fe_xMo_3O_{12}$ (x = 0.4 (■), 0.7 (▲), and 1.2 (●)) obtained from NPD data. The error bars are also presented, but they are too small to be seen.

expansion properties of various compositions. The derived volumetric CTE values of $Sc_{1.6}Fe_{0.4}Mo_3O_{12}$ and $Sc_{0.8}Fe_{1.2}Mo_3O_{12}$ from Rietveld refinement are −2.48 × 10^{-6} °C^{-1} and 3.50 × 10^{-6} °C^{-1}, respectively, whereas the volume of $Sc_{1.3}Fe_{0.7}Mo_3O_{12}$ derived from Rietveld refinement is almost unchanged at 250−800 °C, indicating a near zero thermal expansion with an α_v of 0.28 × 10^{-6} °C^{-1}. The axial and volumetric CTEs for $Sc_{2-x}Fe_xMo_3O_{12}$ (x = 0.0, 0.4, 0.7, and 1.2) are shown in Table 1. The α_a, α_b, and α_c increase as Fe content increases, and α_v increases from negative to positive as a result.

Table 1. Axial and Volumetric CTEs of Orthorhombic $Sc_{2-x}Fe_xMo_3O_{12}$

compound	α_a(×10^{-6} °C^{-1})	α_b(×10^{-6} °C^{-1})	α_c(×10^{-6} °C^{-1})	α_v(×10^{-6} °C^{-1})
x = 0.0 (25−800 °C)[19]	−6.41	4.07	−4.65	−7.00
x = 0.4 (25−800 °C)	−5.16	6.10	−3.39	−2.48
x = 0.7 (150−800 °C)	−3.99	6.27	−2.14	0.28 (250−800 °C)
x = 1.2 (250−800 °C)	−2.85	7.24	−0.87	3.50

3.3.2. Neutron Powder Diffraction Studies. Neutron diffraction can provide good structural information on compounds containing light atoms, such as O, because of the irregular neutron scattering length variation with atomic number Z; that is, the neutron scattering length of O is comparable with those of the heavy atoms such as Mo, Fe, and Sc. Therefore, NPD can be used to determine the crystal structure especially the O positions with high reliability. Representatives of neutron refinement plots for $Sc_{1.3}Fe_{0.7}Mo_3O_{12}$ at 27 °C (monoclinic phase) and 127 °C (orthorhombic phase) are shown in Figure 3. Atomic positions for the orthorhombic phase at the representative temperatures 127 and 427 °C are listed in Table 2. The shift in atomic positions is small for different temperatures.

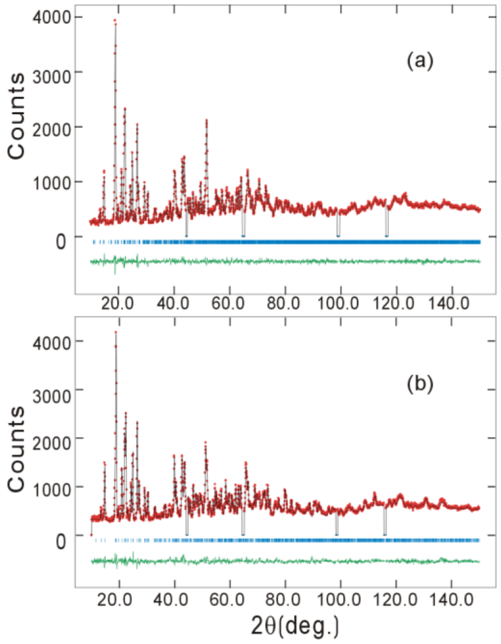

Figure 3. Representative neutron Rietveld plots for $Sc_{1.3}Fe_{0.7}Mo_3O_{12}$ at 27 °C, (a) monoclinic structure, and 127 °C, (b) orthorhombic structure. The excluded regions are due to the peaks from the Al sample holder. The vertical lines indicate the Bragg positions. The noisy line below observed and calculated patterns shows the difference between the observed and calculated intensities.

Table 2. Atomic Coordinates for $Sc_{1.3}Fe_{0.7}Mo_3O_{12}$ at 127 and 427 °C Obtained from NPD Data

	x	y	z	U_{iso} × 100
		127 °C		
Sc1/Fe1	0.4649(2)	0.3800(2)	0.2483(4)	1.52(5)
Mo1	0.250 000	0.000 000	0.4712(4)	2.0(2)
Mo2	0.1190(4)	0.3551(3)	0.3947(5)	1.7(1)
O1	0.0915(5)	0.1427(5)	0.0812(5)	2.7(1)
O2	0.1285(7)	0.0640(4)	0.3678(7)	4.6(2)
O3	0.0068(6)	0.2643(4)	0.3227(6)	4.0(2)
O4	0.3342(6)	0.4112(4)	0.0803(5)	3.3(2)
O5	0.0757(6)	0.4722(4)	0.3243(6)	3.4(2)
O6	0.2949(7)	0.3300(4)	0.3616(6)	3.3(2)
		427 °C		
Sc1/Fe1	0.4676(3)	0.3810(2)	0.2483(5)	1.96(6)
Mo1	0.250 000	0.000 000	0.4744(8)	2.8(2)
Mo2	0.1151(5)	0.3550(4)	0.3942(6)	2.6(1)
O1	0.0932(6)	0.1418(6)	0.0791(6)	3.7(2)
O2	0.1372(8)	0.0658(5)	0.3659(8)	5.3(2)
O3	0.0079(8)	0.2633(5)	0.3232(8)	5.1(2)
O4	0.3408(7)	0.4131(5)	0.0807(7)	4.2(2)
O5	0.0715(7)	0.4726(5)	0.3223(8)	5.2(2)
O6	0.2925(8)	0.3341(5)	0.3614(7)	4.6(2)

The temperature dependence of unit cell parameters and the volume of orthorhombic $Sc_{2-x}Fe_xMo_3O_{12}$ (x = 0 and 0.7) derived from neutron data is shown in Figure 4. The precisely measured lattice parameters from NPD with very small deviations warrant a reliable determination of CTE values. There is some difference in the unit cell volumes measured from XRD (~1175 Å³) and NPD (~1178 Å³) for $Sc_{1.3}Fe_{0.7}Mo_3O_{12}$ due to the systematic errors from different instruments, temperature controllers, and high-temperature furnaces. Nonetheless, the trend of the unit cell parameter changes and the volumetric CTE calculated for the composition x = 0.7, i.e., $Sc_{1.3}Fe_{0.7}Mo_3O_{12}$, indicated a near zero thermal

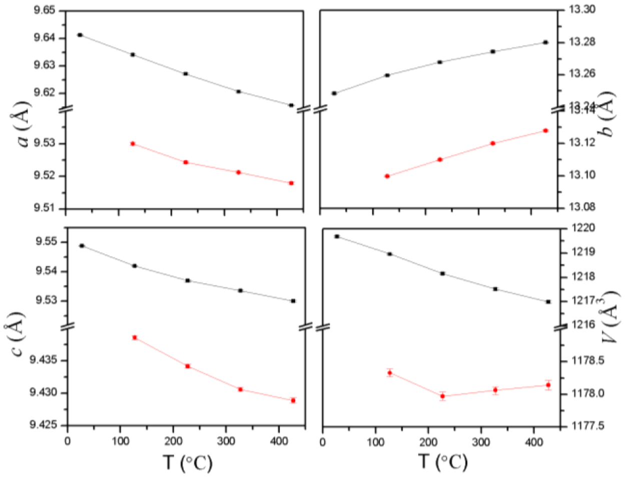

Figure 4. Variation of lattice parameters and volume as a function of temperature for orthorhombic $Sc_{2-x}Fe_xMo_3O_{12}$ (x = 0 (■) and 0.7 (●)) derived from neutron data.

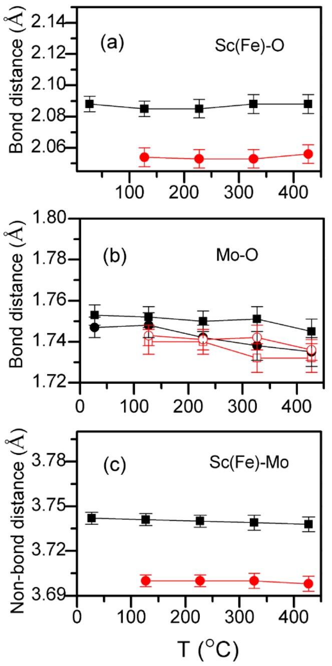

Figure 5. Average bond distances of (a) Sc(Fe)–O (x = 0 (■) and 0.7 (●)), (b) Mo–O (x = 0 (Mo1 ■, Mo2 ●) and 0.7 (Mo1 □, Mo2 ○)), and (c) Sc(Fe)–Mo (x = 0 (■) and 0.7 (●)) in $Sc_{2-x}Fe_xMo_3O_{12}$ as a function of temperature.

expansion from both measurement techniques. A linear contraction of cell parameters a and c and an expansion of b are observed with increasing temperature. The relative magnitudes of the lattice constant changes lead to a negative thermal expansion of $Sc_2Mo_3O_{12}$ with a volumetric CTE of -5.56×10^{-6} °C^{-1}, different from previous results,[17,19] which might be due to the different temperature ranges. The volume of $Sc_{1.3}Fe_{0.7}Mo_3O_{12}$ remains almost unchanged between 227 and 427 °C ($\alpha_v = 0.65 \times 10^{-6}$ °C^{-1}). The ZET phenomenon is consistent with the HTXRD result, which was measured at a higher temperature range.

To investigate the effect of Fe substitution on the structure and thermal expansion, the variations in bond distances and bond angles were systematically studied. Sc–O bonds exhibit minor deviations from the octahedral symmetry, ranging from 2.07(1) Å (Sc–O3, 227 °C) to 2.11(1) Å (Sc–O6, 327 °C) for $Sc_2Mo_3O_{12}$ and 2.03(1) Å (Sc(Fe)–O1, 327 °C) to 2.08(1) Å (Sc(Fe)–O5, 427 °C) for $Sc_{1.3}Fe_{0.7}Mo_3O_{12}$. The average Sc(Fe)–O distance remains essentially unchanged as a function of temperature (shown in Figure 5a). Fe substitution for Sc leads to a contraction of the average bond distances, which is expected because of the smaller size of Fe^{3+} than Sc^{3+}.

Mo–O bonds also exhibit small deflections from the ideal tetrahedron, ranging from 1.72(1) Å (Mo2–O6, 327 °C) to 1.76(1) Å (Mo1–O4, 127 °C) for $Sc_2Mo_3O_{12}$ and 1.72(1) Å (Mo2–O3, 427 °C) to 1.78(1) Å (Mo2–O1, 327 °C) for $Sc_{1.3}Fe_{0.7}Mo_3O_{12}$. The average Mo–O distance shows a contraction with increasing temperature (shown in Figure 5b); this finding is in agreement with previous studies, which showed that the W–O and Mo–O bond lengths undergo reduction upon heating.[4,25,26] However, this apparent contraction is not the intrinsic reason for the NTE as discussed below.

The orthorhombic structure of $A_2Mo_3O_{12}$ consists of a corner-sharing network of AO_6 octahedra and MoO_4 tetrahedra (see Figure S1). This structure is a relatively open framework with A and Mo atoms linked by two coordinated oxygen atoms. The mechanism of NTE of orthorhombic $A_2Mo_3O_{12}$ has been attributed to the rocking motion of the polyhedra related to the transverse vibrations of the 2-fold-coordinated oxygen (see Figure S2).[1,2] This vibrational motion of oxygen will lead to the apparent decrease in M–O distance.[4,27] If there is no obvious variation in the real M–O distance with temperature, the apparent Sc(Fe)–O and Mo–O are expected to decrease equally. In fact, no change in the average apparent Sc(Fe)–O distance is observed. The previous study[28] on the correlation between bond strength and the thermal vibrations of bonds indicated that very strong bonds such as Mo–O are expected to remain unchanged with increasing temperature, whereas the weaker Sc(Fe)–O bond should have a slight increase. However, no expansion of Sc(Fe)–O bonds was detected in the present study. This suggested that the vibrational thermal motion of oxygen might compensate for the expected thermal expansion of Sc(Fe)–O bond lengths.

Orthorhombic $Sc_{1.3}Fe_{0.7}Mo_3O_{12}$ and $Sc_2Mo_3O_{12}$ have the same structure, but the thermal expansion behaviors are different. Herein, one necessary factor for NTE should be pointed out, that is, the slight distortion of the polyhedron.[29,30] Marinkovic et al.[31] have quantitatively investigated polyhedron distortion using the inherent volume distortion parameter (υ) of AO_6, and they observed that this parameter is strongly correlated with the NTE in the $A_2M_3O_{12}$ family. Previous studies have validated that the NTE coefficient is more negative for $Y_2W_3O_{12}$[25] than $Sc_2W_3O_{12}$.[4] The calculated υ of the YO_6 polyhedron in $Y_2W_3O_{12}$ is larger than that of the ScO_6 polyhedron in $Sc_2W_3O_{12}$,[31] which is expected based on the larger radius of Y^{3+} than Sc^{3+}. This result indicates that for the AO_6 polyhedron with a small central cation, the oxygen–oxygen repulsive interaction increases and slight distortions are blocked. The polyhedron volume distortions υ of AO_6 in $Sc_{1.3}Fe_{0.7}Mo_3O_{12}$ and $Sc_2Mo_3O_{12}$ calculated using the program IVTON[32] at different temperatures are given in Figure 6. Due to the substitution of smaller Fe^{3+}, the υ of $Sc(Fe)O_6$ in $Sc_{1.3}Fe_{0.7}Mo_3O_{12}$ is smaller than that of ScO_6 in $Sc_2Mo_3O_{12}$. The υ of AO_6 in $Sc_{2-x}Fe_xMo_3O_{12}$ increases with temperature, as observed in other $A_2M_3O_{12}$ families,[31] which indicates that the polyhedra are semirigid. In $Sc_2Mo_3O_{12}$, υ of ScO_6 increases

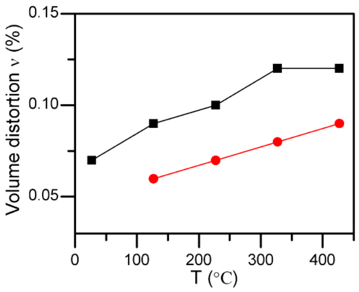

Figure 6. Volume distortion parameter of AO_6 polyhedra in $Sc_{2-x}Fe_xMo_3O_{12}$ ($x = 0$ (■) and 0.7(●)) as a function of temperature.

from 0.07% to 0.12% from 27 to 427 °C. The smaller υ of $Sc(Fe)O_6$ in $Sc_{1.3}Fe_{0.7}Mo_3O_{12}$ inhibits the NTE and leads to its near zero thermal expansion.

The negative or zero thermal expansion of orthorhombic $Sc_{2-x}Fe_xMo_3O_{12}$ could be manifested as changes in the Sc(Fe)−Mo nonbond distances and certain Sc(Fe)−O−Mo bond angles. The average Sc(Fe)−Mo nonbond distances in $Sc_{2-x}Fe_xMo_3O_{12}$ ($x = 0.0$ and 0.7) obtained upon increasing the temperature are shown in Figure 5c. The Sc(Fe)−Mo distance as a function of temperature shows a noticeable reduction for $Sc_2Mo_3O_{12}$, but remains constant for $Sc_{1.3}Fe_{0.7}Mo_3O_{12}$. From the above discussion on the AO_6 polyhedron distortion, it can be rationalized that the transverse vibrations of oxygen are attenuated in $Sc_{1.3}Fe_{0.7}Mo_3O_{12}$ owing to the rigidity of the $Sc(Fe)O_6$ octahedron; as a result, the mean nonbond distance is almost unchanged in $Sc_{1.3}Fe_{0.7}Mo_3O_{12}$ with increasing temperature. In addition, transverse vibrations of oxygen are not strong enough in $Sc_{1.3}Fe_{0.7}Mo_3O_{12}$ to provoke a negative CTE. However, transverse vibrations of oxygen could happen in $Sc_2Mo_3O_{12}$ due to the slight distortion of the ScO_6 octahedron, leading to the NTE property of $Sc_2Mo_3O_{12}$.

Variations in Sc(Fe)−O−Mo bond angles with temperature are shown in Figure 7. The variations in Sc−O−Mo bond angles in $Sc_2Mo_3O_{12}$ are similar to those reported for Sc−O−W in $Sc_2W_3O_{12}$ (also reported in $Y_2W_3O_{12}$, $Al_2W_3O_{12}$, $Y_2Mo_3O_{12}$, $Er_2Mo_3O_{12}$).[4,25,26] The Sc−O2−Mo1 angle significantly decreases, whereas the angles Sc−O4−Mo1 and Sc−O6−Mo2 linearly increase over the studied temperature range. The variations in Sc−O1−Mo2, Sc−O3−Mo2, and Sc−O5−Mo2 are small over the entire temperature range. Fe doping at the Sc site in $Sc_{1.3}Fe_{0.7}Mo_3O_{12}$ obviously expands the Sc(Fe)−O5−Mo2 and Sc(Fe)−O2−Mo1 bond angle and reduces Sc(Fe)−O1−Mo2 and Sc(Fe)−O3−Mo2. The trends of variations in Sc(Fe)−O−Mo angles (for O1, O2, O4, and O6) in $Sc_{1.3}Fe_{0.7}Mo_3O_{12}$ are similar to those in $Sc_2Mo_3O_{12}$. However, the bond angles of Sc(Fe)−O−Mo angles (for O3 and O5) in $Sc_{1.3}Fe_{0.7}Mo_3O_{12}$ vary in a different manner from those in $Sc_2Mo_3O_{12}$; these angles slightly increase in $Sc_{1.3}Fe_{0.7}Mo_3O_{12}$, but decrease little in $Sc_2Mo_3O_{12}$.

In order to investigate the correlation between the thermal displacements of the oxygen atoms and (1) their related bridging angles and (2) the thermal variation of cell parameters, the distortions of the bridging oxygen atoms in $Sc_2Mo_3O_{12}$ have been calculated by the program AMPLIMODES[33] and refined using Fullprof. The orthorhombic structure data at 427 °C are input as the "high-symmetry structure", and the "more distorted structure" are those orthorhombic data at low temperature (Table S1). Since space group *Pnca* is not the standard setting in the program AMPLIMODES, the input structure data are transformed to *Pbcn*. The relationship between *Pbcn* (a', b', and c') and *Pnca* (a, b, and c) are as follows: $a' = b$; $b' = c$; $c' = a$. The structure can be described with the distortion mode GM1+, which was calculated from the AMPLIMODES program. The calculated global amplitude of the GM1+ mode is 0.399 Å at 27 °C. The AMPLIMODES results indicate that there are 25 total distortion modes (GM1+), three modes for each atom at the general position and one for each atom at the special Wyckoff position (e.g., Mo1 atom at the 4*c* site) (Table S2). The thermal displacements of atoms O2 and O4 are relatively large, whereas those of O1, O3, and O5 are small.

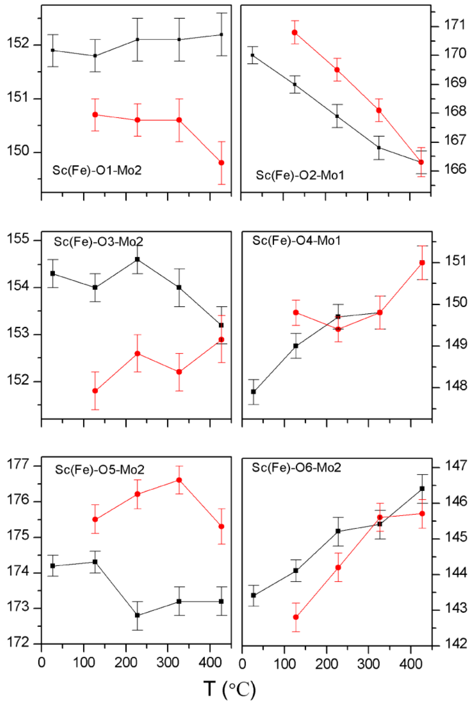

Figure 7. Temperature variations of Sc(Fe)−O−Mo bond angles in $Sc_{2-x}Fe_xMo_3O_{12}$ ($x = 0$ (■) and 0.7 (●)).

The thermal distortions of bridging oxygen atoms in $Sc_2Mo_3O_{12}$ at 27 °C with respect to the structure at 427 °C are shown in Figure 8 and Figure 9, where the arrows indicate the direction and magnitude of the oxygen displacements on cooling. From Figure 8b, it can be observed that the Sc and Mo1 are connected by O2 and O4, forming an eight-membered ring, and each ring is linked by Mo1, forming a chain of rings spreading along the *c*-axis, whereas each chain of rings is separated in the *a* direction. From the directions of the oxygen displacements, the angles Sc−O2−Mo1 and Sc−O4−Mo1 will increase and decrease upon cooling, respectively, which is in accordance with their thermal variations as shown in Figure 7. Increasing of the Sc−O2−Mo1 angle cooperates with decreasing of Sc−O4−Mo1, leading to the expansion of the c' (a) parameter. However, such cation−anion rings involving O2 and O4 atoms, highlighted in Figure 8a, are not connected in the *b* direction; therefore, the origin of the lattice expansion b' (c) in this direction is unclear.

From Figure 9a, cation−anion network rings involving O5 and O6 (highlighted in yellow) are connected along the *c*-axis through Mo2−O1−Sc bridges, and these rings are connected through Mo2−O3−Sc bridges in the *a* direction. The decrease of the Sc−O6−Mo2 angle and the increase of the Sc−O2−Mo1 angle (Figure 8a) will affect the changes in the c' (a)

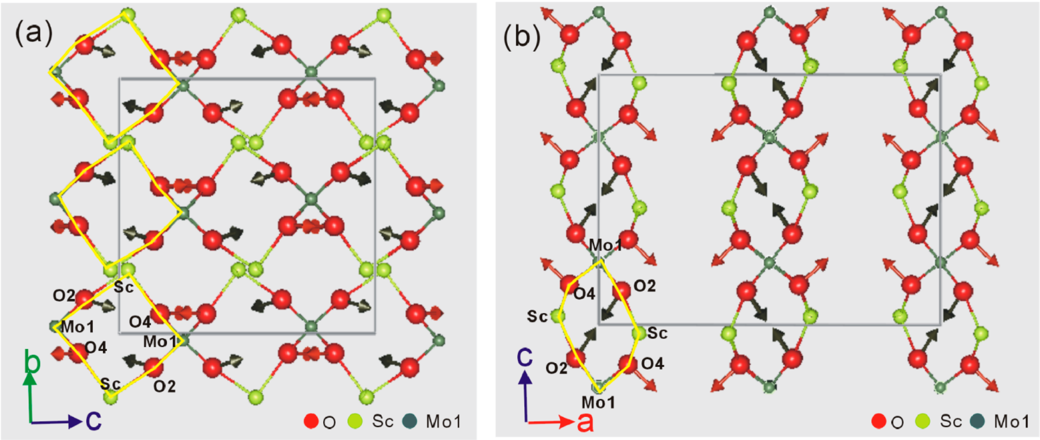

Figure 8. Displacements of oxygen atoms in the structure of $Sc_2Mo_3O_{12}$. $Mo(2)O_4$ tetrahedra were omitted for clarity. (a) *a*-axis view and (b) *b*-axis view. The black and red arrows indicate the direction and magnitude of the displacement of O2 and O4, respectively (figures created using Fullprof Studio).

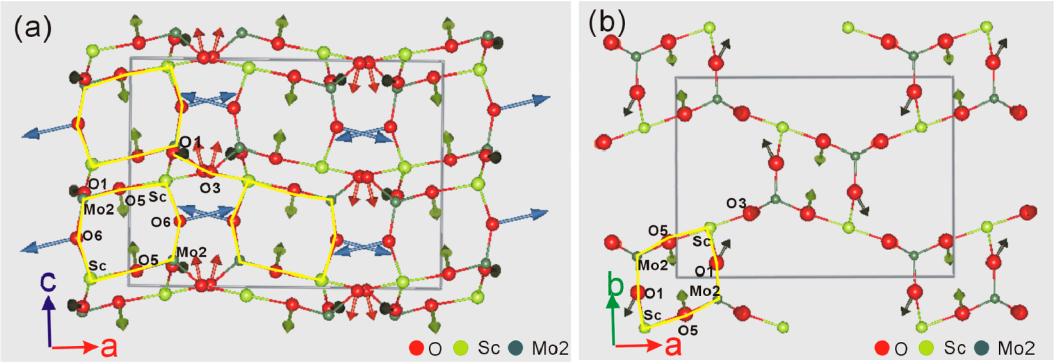

Figure 9. Displacements of oxygen atoms in the structure of $Sc_2Mo_3O_{12}$. $Mo(1)O_4$ tetrahedra were omitted for clarity. (a) *b*-axis view and (b) *c*-axis (the atoms have been halved along the c-axis for clarity) view. The black, red, green, and blue arrows indicate the direction and magnitude of the thermal displacement of O1, O3, O5, and O6, respectively. The magnitudes of the displacement vectors have been magnified 2 times for better view (figures created using Fullprof Studio).

parameter in an opposite way, and the net effect in the present system will result in an expansion in the c' (a) parameter. From Figure 9b, the cation−anion network rings involving O1 and O5 are connected through O3 in the a−b plane. Since the displacements of atoms O1, O3, and O5 are small, their contribution in the thermal variations of cell parameters is insignificant.

4. CONCLUSIONS

High-temperature XRD and NPD results indicate that the volumetric CTE of $Sc_{2-x}Fe_xMo_3O_{12}$ varies from negative to positive with increasing Fe content. $Sc_{1.3}Fe_{0.7}Mo_3O_{12}$ exhibits near zero thermal expansion, and the calculated volumetric TECs derived from XRD and NPD are 0.28×10^{-6} °C^{-1} (250−800 °C) and 0.65×10^{-6} °C^{-1} (227−427 °C), respectively. With the precise oxygen positions determined by neutrons, we have determined accurately the variations of the bond distances, bond angles, inherent volume distortion parameter, and the nonbond distances in $Sc_2Mo_3O_{12}$ and $Sc_{1.3}Fe_{0.7}Mo_3O_{12}$. Our results suggest some special structure parameters such as Sc(Fe)−O5−Mo2 and Sc(Fe)−O3−Mo2 bond angles, the Sc(Fe)−Mo nonbond distance, and the inherent volume distortion parameter are closely related to the NTE and zero thermal expansion (ZTE) feature observed in $Sc_2Mo_3O_{12}$ and $Sc_{1.3}Fe_{0.7}Mo_3O_{12}$. The magnitudes of oxygen distortions indicate the variation of the bond angles and unit cell parameters in different axial directions.

■ ASSOCIATED CONTENT

Ⓢ Supporting Information

Tables of structure and the refined amplitudes of the irreducible representation distortion presented in the distorted structures at different temperatures. This material is available free of charge via the Internet at http://pubs.acs.org.

■ AUTHOR INFORMATION

Corresponding Authors

*E-mail: mmwu@ciae.ac.cn.
*E-mail: dfchenciae@126.com.

Notes

The authors declare no competing financial interest.

■ ACKNOWLEDGMENTS

This work was supported by the National Natural Science Foundation of China (NSFC) (Grant No. 10905095) and 973 Programs (2010CB833101).

■ REFERENCES

(1) Sleight, A. W. *Annu. Res. Mater. Sci.* **1998**, *28*, 29−43.
(2) Evans, J. S. O. *J. Chem. Soc., Dalton Trans.* **1999**, 3317−3326.

(3) Evans, J. S. O.; Mary, T. A.; Vogt, T.; Subramanian, M. A.; Sleight, A. W. *Chem. Mater.* **1996**, *8*, 2809−2823.
(4) Evans, J. S. O.; Mary, T. A.; Sleight, A. W. *J. Solid State Chem.* **1998**, *137*, 148−160.
(5) Evans, J. S. O.; Mary, T. A.; Sleight, A. W. *Phys. B (Amsterdam, Neth.)* **1998**, *241−243*, 311−316.
(6) Takenaka, K.; Asano, K.; Misawa, M.; Takagi, H. *Appl. Phys. Lett.* **2008**, *92*, 011927.
(7) Wang, C.; Chu, L. H.; Yao, Q. R.; Sun, Y.; Wu, M. M.; Ding, L.; Yan, J.; Na, Y. Y.; Tang, W. H.; Li, G. N.; et al. *Phys. Rev. B* **2012**, *85*, 220103.
(8) Chen, J.; Xing, X. R.; Sun, C.; Hu, P.; Yu, R. B.; Wang, X. W.; Li, L. H. *J. Am. Chem. Soc.* **2008**, *130*, 1144−1145.
(9) Goodwin, A. L.; Calleja, M.; Conterio, M. J.; Dove, M. T.; Evans, J. S. O.; Keen, D. A.; Peters, L.; Tucker, M. G. *Science* **2008**, *319*, 794−797.
(10) Wang, X. W.; Huang, Q. Z.; Deng, J. X.; Yu, R. B.; Chen, J.; Xing, X. R. *Inorg. Chem.* **2011**, *50*, 2685−2690.
(11) Sleight, A. W.; Brixner, L. J. *J. Solid State Chem.* **1973**, *7*, 172−174.
(12) Mary, T. A.; Sleight, A. W. *J. Mater. Res.* **1999**, *14*, 912−915.
(13) Cheng, Y. Z.; Wu, M. M.; Peng, J.; Xiao, X. L.; Li, Z. X.; Hu, Z. B.; Kiyanagi, R.; Fieramosca, J. S.; Short, S.; Jorgensen, J. *Solid State Sci.* **2007**, *9*, 693−698.
(14) Ari, M.; Jardim, P. M.; Marinkovic, B. A.; Rizzo, F.; Ferreira, F. F. *J. Solid State Chem.* **2008**, *181*, 1472−1479.
(15) Wu, M. M.; Xiao, X. L.; Hu, Z. B.; Liu, Y. T.; Chen, D. F. *Solid State Sci.* **2009**, *11*, 325−329.
(16) Li, Z. Y.; Song, W. B.; Liang, E. J. *J. Phys. Chem. C* **2011**, *115*, 17806−17811.
(17) Evans, J. S. O.; Mary, T. A. *Int. J. Inorg. Mater.* **2000**, *2*, 143−151.
(18) Chen, H. Y. *Mater. Res. Bull.* **1979**, *14*, 1583−1590.
(19) Wu, M. M.; Peng, J.; Han, S. B.; Hu, Z. B.; Liu, Y. T.; Chen, D. F. *Ceram. Int.* **2012**, *38*, 6525−6529.
(20) Rodriguez-Carjaval, J. *FULLPROF, Program for Rietveld Analysis of X-ray and Neutron Powder Diffraction Patterns*; Laboratoire Leon Brillouin (CEACNRS): France, 2005.
(21) Larson, A. C.; Von Dreele, R. B. In *General Structure Analysis System (GSAS)*; Larson, A. C.; Von Dreele, R. B., Eds.; Los Alamos National Laboratory: LAUR, 2000.
(22) Sleight, A. W.; Brixner, L. J. *J. Solid State Chem.* **1973**, *7*, 172−174.
(23) Evans, J. S. O.; Mary, T. A.; Sleight, A. W. *J. Solid State Chem.* **1997**, *133*, 580−583.
(24) Tyagi, A. K.; Achary, S. N.; Mathews, M. D. *J. Alloys Compd.* **2002**, *339*, 207−210.
(25) Woodcock, D. A.; Lightfoot, P.; Ritter, C. *J. Solid State Chem.* **2000**, *149*, 92−98.
(26) Guzman-Afonso, C.; Gonzalez-Silgo, C.; Gonzalez-Platas, J.; Torres, M. E.; Lozano-Gorrin, A. D.; Sabalisck, N.; Sanchez-Fajardo, V.; Campo, J.; Rodriguez-Carvajal, J. *J. Phys: Condens. Matter* **2011**, *23*, 325402.
(27) Weller, M. T.; Henry, P. F.; Wilson, C. C. *J. Phys. Chem. B* **2000**, *104*, 12224−12229.
(28) Hazen, R. M.; Prewitt, C. T. *Am. Mineral.* **1977**, *62*, 309−315.
(29) Forster, P. M.; Yokochi, A.; Sleight, A. W. *J. Solid State Chem.* **1998**, *140*, 157−158.
(30) Forster, P. M.; Sleight, A. W. *Int. J. Inorg. Mater.* **1999**, *1*, 123−127.
(31) Marinkovic, B. A.; Ari, M.; deAvillez, R. R.; Rizzo, F.; Ferreira, F. F.; Miller, K. J.; Johnson, M. B.; White, M. A. *Chem. Mater.* **2009**, *21*, 2886−2894.
(32) Balic Zunic, T.; Vickovic, I. *J. Appl. Crystallogr.* **1996**, *29*, 305.
(33) Orobengoa, D.; Capillas, C.; Aroyo, M. I.; Manuel Perez-Mato, J. *J. Appl. Crystallogr.* **2009**, *42*, 820−833.